Plutonium retention mechanisms by magnetite under anoxic conditions: Entrapment versus sorption

Dumas, T.; Fellhauer, D.; Schild, D.; Gaona, X.; Altmaier, M.; Scheinost, A.;

Originally published:

July 2019

ACS Earth and Space Chemistry 3(2019)10, 2197-2206

DOI: https://doi.org/10.1021/acsearthspacechem.9b00147

Perma-Link to Publication Repository of HZDR:

https://www.hzdr.de/publications/Publ-29235

Plutonium retention mechanisms by magnetite under anoxic conditions: Entrapment versus sorption

*Thomas Dumas[1,2,5], David Fellhauer[3,4], Dieter Schild[3], Xavier Gaona[3], Marcus Altmaier[3], Andreas C. Scheinost[1,2**]*

[1] The Rossendorf Beamline at ESRF (Grenoble, France)

[2] HZDR Inst. of Resource Ecology (Dresden, Germany)

[3] KIT Inst. f. Nuclear Waste Disposal (Karlsruhe, Germany)

[4] JRC Karlsruhe (Karlsruhe, EU)

[5] French Nuclear and Alternative Energies Commission CEA Nuclear Energy Division – CEA Marcoule Research Department of Mining and Fuel Recycling ProCesses (DMRC)- Site de Marcoule, BP17171, 30207 Bagnols sur Cèze, France.

**Corresponding author: scheinost@esrf.fr

KEYWORDS. Plutonium, magnetite, redox, XAFS spectroscopy, radioactive waste.

ABSTRACT: (319 words): The reliable prediction of possible plutonium migration into the geological environment is crucial for the safety assessment of radioactive waste repositories. Fe(II)-bearing corrosion products like magnetite, which form on the surface of steel waste containers, can effectively contribute to the retardation of the potential radionuclide release by sorption and redox reactions, eventually followed by formation of secondary precipitates. A retardation process even more efficient - especially when considering the required long time scales for nuclear waste reposition - is structural incorporation by magnetite, as has been demonstrated for Tc and U. Here we show that this mechanism might not be as relevant for Pu retention: after a rapid reduction of Pu(V) to Pu(III) in acidic Fe(II)/Fe(III) solution, base-induced magnetite precipitation ($pH_{exp} \approx 12.5$) leads only to a partial (≈ 50%) incorporation, while the other half remains at the surface by forming tridentate sorption complexes. Neither solid nor sorbed Pu(IV) species were observed in the starting solution and after precipitation. With Fe(II)-inforced re-crystallization at $pH_{exp} = 6.5$, a process potentially mimicking long-term, thermodynamically controlled aging, the equilibrium between both Pu species is even further shifted towards the sorption complex. A detailed analysis of the incorporated species by Pu L_{III}-edge X-ray absorption fine-structure (XAFS) spectroscopy shows a pyrochlore-like coordination environment (split eight-fold oxygen coordination shell with Pu-O distances of 2.22 and 2.45 Å, and an edge-sharing linkage to Fe-octahedra with Pu-Fe distances of 3.68 Å), which is embedded in the magnetite matrix (Pu-Fe distances of 3.93, 5.17 and 5.47 Å). This suggests that the reason for the partial incorporation is the structural incompatibility of the large Pu(III) ion for the octahedral Fe site in magnetite. The adoption of a pyrochlore-like local environment within the magnetite long-range structure might be induced by the rapid coprecipitation rather than being a thermodynamically stable state (kinetic entrapment). For the sake of conservatism, safety assessments should rely on the formation of the Pu(III) sorption complex only.

INTRODUCTION

As the major chemical and radiotoxic transuranium element in civil and military nuclear waste, plutonium has to be considered as a major issue for the long-term safety of nuclear waste repositories. Unlike the lanthanides, and more similar to its early actinide neighbors uranium and neptunium, plutonium can occur in several oxidation states within the water stability field, including III, IV, V and VI.[1] Given the complexity to work with Pu, only few studies have been conducted to elucidate potential links between Pu oxidation state, its association with minerals in the sediments, and the desorption or migration behaviour. In lysimeter experiments with natural sediments,[2-4] all oxidation states were observed in the aqueous phase, while Pu(IV) prevailed in association with the solid phase and increased with time. Pu solubility increased under subsequent oxidative conditions, presumably through partial oxidation of Pu(IV) to more soluble Pu(V), and/or through lowering the pH by one unit in line with the equilibrium solubility of PuO_2. After sorption to natural tuff, Pu(V) and Pu(VI) was found to be associated with manganese oxide and clay minerals, but not with iron oxide.[5] In contrast, Pu is associated with iron (hydr)oxide colloids at the Nevada Test Site (USA) and at the Mayak Production Association (Russian Federation), thereby undergoing colloid-facilitated transport.[6, 7]. Processes influencing Pu migration and uptake by biota, including complexation and redox reactions of Pu with humic substances, peptides, and proteins, with bacteria and with a range of minerals, have been predominately investigated under oxic conditions.[8-13] In the case of the deep underground repositories foreseen by several countries for disposal of nuclear waste, however, anoxic conditions will develop soon after closure of the mine shafts. In addition, radiolytic water dissociation under near-field conditions will produce hydrogen gas, further lowering the redox potential.[14] Under such conditions, the first technical barrier consisting of stainless-steel casks will corrode over the geological time scales to be considered. Depending on the technical backfill material (clays like bentonite), the natural bedrock (e.g. clay, granite,

or salt) and the nature of the eventually penetrating groundwater, a range of Fe(II)-bearing minerals may form during the corrosion processes, including oxides like magnetite (Fe_3O_4), sulfides like mackinawite (FeS), (hydroxo) carbonates like siderite ($FeCO_3$) and chukanovite ($Fe_2(OH)_2(CO_3)$), as well as Fe-rich clays like nontronite.[15-18] The low redox potential along with the catalytic effect of these Fe(II)-bearing minerals has been shown to greatly reduce the mobility of redox-reactive actinides (U, Np) and fission products (Se, Tc) by sorption and reduction processes producing solid compounds with very low solubility like $U^{IV}O_2$, [19-23] $Np^{IV}O_2$,[24-26] _ENREF_16 FeSe,[27-29] $Tc^{IV}O_2$ [22, 30, 31] _ENREF_30 While formation of PuO_2 with similarly low solubility has also been observed during mineral sorption reactions under both oxic and anoxic conditions,[32-34], Pu may also be further reduced to the oxidation state III, where it occurs as aquo ion with high solubility in acidic to weakly alkaline solutions. Note the similar geochemical behavior of Pu(III) with its next actinide neighbors, Am and Cm, which are prevalently trivalent. Formation of Pu(III) by magnetite has in fact been confirmed by Kirsch et al. under anoxic conditions similar to those expected for deep underground repositories.[35] A very stable Pu(III) surface complex was identified, where mononuclear Pu(III) atoms are linked via three oxygen atoms to three edge-sharing FeO_6-octahedra at the magnetite {111} faces. This surface complex has a high affinity towards the magnetite surface as expressed by Pu concentrations below 10^{-9} M (i.e. the detection limit of laser scintillation counting for ^{242}Pu).

The release of Fe(II) from hydrogen-driven steel corrosion and subsequent precipitation of magnetite may create a highly dynamic system where one could envision that Pu is incorporated by magnetite following either a coprecipitation process or by overgrowth of an already existing magnetite surface with adsorbed Pu. Such a process has been observed for instance for Tc(IV) and Sn(IV), two cations with ionic radii (0.65 Å and 0.69 Å, respectively) similar to those of Fe(II) or Fe(III) (0.78 Å and 0.65 Å respectively), which therefore can easily replace Fe in octahedral sites.[31, 36, 37] _ENREF_22 More surprisingly from a crystal-chemical point of view,

this has also been demonstrated for the larger actinide U.[38-40] In this case, U is preferentially incorporated in its pentavalent oxidation state, by adopting a uranate-type local structure characterized by relaxation of the multiply bonded "-yl" oxygen ligands.

The large ionic radius of trivalent Pu (1.00 Å), along with that of Am (0.975 Å) and Cm (0.95 Å), however, seems to be too large to be hosted by the octahedral site of Fe with oxidation state of 2.5 and an expected ionic radius of 0.713 Å (0.645+0.78)/2). Nevertheless, a significant body of work shows incorporation of early trivalent lanthanides, which have ionic radii similar to those of the early actinides, by magnetite through a variety of synthesis procedures including bacterial processes. While none of these studies investigated the short-range structure around the lanthanide dopant, the long-range magnetite structure as determined by X-ray diffraction (XRD) was conserved for up to a few percent of dopant.[41-47]

To the best of our knowledge, there are only two recent studies trying to decipher the local structure of Sm and Am doped magnetite by Sm and Am L_{III}-edge XAFS spectroscopy.[48, 49] In both cases doping was successful, while the local structure was in disagreement with a simple Sm/Am-for-Fe substitution at either the octahedral or (even less likely) the tetrahedral site in magnetite. For Am, the short range order probed by EXAFS showed a seven-fold coordination of Am, and Am-Fe distances largely incompatible with the Fe Oh site in magnetite for a fresh sample at pH 5.7, while in a sample aged for two years at pH 12.5, Am was six-fold coordinated more commensurate with the Fe Oh site. Beyond the coordination sphere, however, only 1.5 Fe at 3.40 Å were found, contradicting the substitution into the Fe Oh site, but rather suggesting an alternative local environment. A definitive elucidation was not successful, most likely because of high structural disorder and/or the presence of several local environments, which because of the intrinsically poor resolution of EXAFS (0.1 to 0.2 Å depending on available k-range) are often impossible to discriminate.

The intention of our study was therefore to conduct plutonium/magnetite coprecipitation experiments under anoxic conditions in order to verify, if incorporation may also occur for the redox-susceptible Pu. We used Pu(V) and Pu(III) as initial oxidation states, and followed their oxidation state and local structure during coprecipitation with a mixed Fe(II) and Fe(III) solution using XAFS spectroscopy. In contrast to the previous Am studies, we analyzed the spectroscopic data also with advanced chemometric tools in order to enhance resolution and to discriminate the spectral signal from eventually occurring multiple species. The fresh magnetite coprecipitates were further subjected to Fe(II)-inforced recrystallization, a process potentially mimicking long-term, more thermodynamically controlled aging.[50-53] _ENREF_31

EXPERIMENTAL SECTION

Warning. ^{242}Pu is a highly radiotoxic α-emitter, which must be handled in dedicated laboratory facilities. Its possession and use is subject to strict statutory controls.

General synthesis and analysis conditions. All sample manipulations, including mineral synthesis, washing, preparation of samples for XAS and UV-vis measurements, were carried out under anoxic conditions in argon glove-boxes with <10 ppmv O_2. Samples for XAFS analysis were stored and transported to the synchrotron facility under LN_2 and then measured at 15 K under He atmosphere in a closed-cycle cryostat (CryoVac). Wet chemistry experiments were carried out at room temperature using deionized (18.2MΩ Milli-Q), degassed (O_2 and CO_2 free) water for all purposes.

Preparation of Pu stock solutions. The employed Pu had an isotope composition of 99.4 wt.% ^{242}Pu, 0.58 wt.% ^{239}Pu, 0.005 wt.% ^{238}Pu and 0.005 wt.% ^{241}Pu. Solutions of 1.1 mM Pu(V) and 1.8 mM Pu(III) were prepared electrolytically in 0.5 M NaCl with pH_{exp} 3, and in 0.1 M $NaClO_4$ with pH_{exp} 2 respectively. UV-vis spectroscopy (Fig. SI-1) confirmed the prevalence of the intended oxidation states, and laser scintillation counting (LSC) conducted before and after 10

kD ultrafiltration confirmed the absence of significant amounts of PuO_2 colloids in the stock solutions.

Pu-magnetite coprecipitation. Experiments were conducted with either Pu(V) or Pu(III). Five mL of Fe(II)/Fe(III) solutions were prepared by mixing 2.5 mL of 0.8 $mol.L^{-1}$ $FeCl_2$ solution with 2.5 mL of 1.6 $mol.L^{-1}$ $FeCl_3$ solution and adjusted to pH_{exp} 1.5. Pu(V) or (III) stock solutions were then added to the iron solutions (1.8 ml for Pu(V) and 1.35 mL or 4.72 mL for Pu(III)). UV-vis spectroscopy showed a rapid reduction of Pu(V) to Pu(III) for the first sample (Fig. SI-1) whereas the oxidation state in the two Pu(III) samples remained stable. Further experiments were hence conducted only with the two Pu(III) samples, labelled **Pu-Mag-1300** and **Pu-Mag-4400** with the numbers referring to the target Pu concentration in each sample in µg/g (ppm). Pu coprecipitation with in-situ formed magnetite was induced by rapidly pouring the Fe/Pu solutions into 3.3 mL of a 6 M NaOH solution. pH_{exp} and pe were determined in the black suspensions after 5 min when stable potentials were reached. Pu-Mag-1300 had a pH_{exp} of 12.4 and a pe of −11.1, while Pu-Mag-4400 had a pH_{exp} of 12.5 and a pe of −11.3. After centrifugation, a 1-mL aliquot of the supernatant was separated for further wet chemical analysis. The bottom slurry of magnetite was washed three times with 5 mL of degassed water and after centrifugation the resulting wet paste were isolated for further XRD and XAFS analysis.

Fe-inforced recrystallization procedure. We adapted a procedure from Boland et al.[50] to enhance recrystallization of the iron oxide phases through concomitant Fe(II)/Fe(III) electron exchange, oxide growth and reductive dissolution.[51-54] An aliquot equivalent to ~225 mg of dry **Pu-Mag-1300** and **Pu-Mag-4400** samples was added under stirring into 100 mL of a solution containing 1 mM Fe(II) and buffered at pH_{exp} 6.5 by 50 mM MES buffer (2-(N-morpholino)ethanesulfonic acid). After five days of reaction, the solid samples were

centrifuged and isolated as wet paste for further XAFS and XRD analyses (samples Pu-Mag-1300-rec and Pu-Mag-4400-rec).

Supernatant characterization. The Pu content in the supernatant was measured by LSC. In all four samples, both before and after aging, Pu concentration in the supernatant was below the LSC detection limit ($<10^{-9}$ mol.L^{-1}), i.e. most Pu was associated with the solid phase.

Magnetite characterization. XRD patterns (Cu source) of Pu-Mag-1300, Pu-Mag-4400, Pu-Mag-1300a and Pu-Mag-4400a demonstrate the phase identity and purity by showing only the 220, 311, 400, 511, 440 reflections of the magnetite cubic cell (Fd3m) (Fig. 1). The broadening of the diffraction bands is attributed to the small particle size of the synthetized magnetite. [55, 56] The $Fe(II)/Fe_{tot}$ ratio in the two non-aged magnetite samples was determined by dissolving the solid samples and then determining the Fe(II) concentration spectrophotometrically[57] in ultrafiltrated (10 kD) aliquots before (=structural Fe(II)) and after Fe reduction with NH_2OH-HCl (=structural total Fe). The structural $Fe(II)/Fe_{tot}$ ratios of 0.32 (Pu-Mag-1300) and 0.30 (Pu-Mag-4400) were close to the ideal ratio of stoichiometric magnetite (0.33).

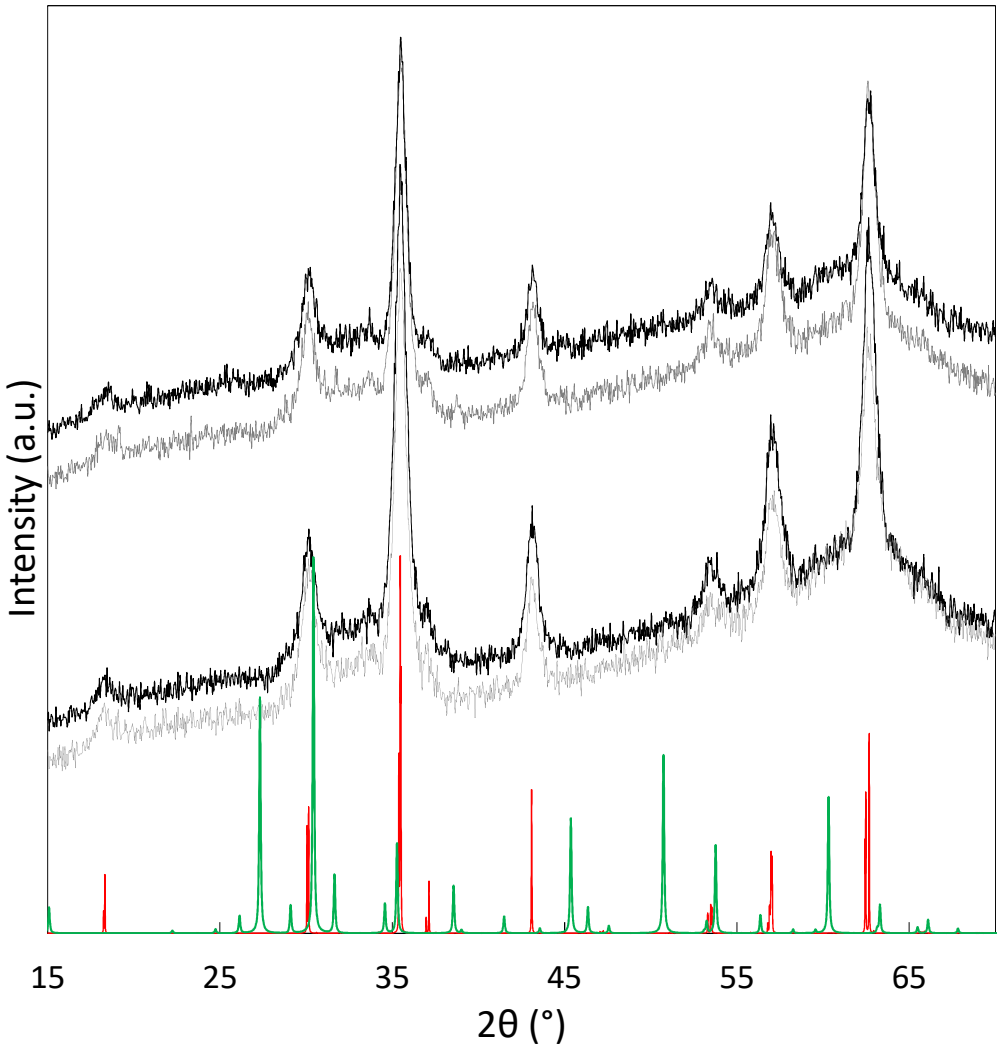

Fig. 1. Powder-XRD for samples Pu-mag-1300, Pu-mag-1300-rec, Pu-mag-4400 and Pu-mag-4400-rec (from top the bottom) and calculated powder pattern from Wright et al.[58] for magnetite (red line) and for the Europium pyrochlore type structure from Chtoun et al.[59] (green line).

X-ray photoelectron spectroscopy (XPS). A PHI model V5000-K VersaProbe II was used with monochromatised Al Kα radiation (1486.7 eV). Calibration of the binding energy scale of the spectrometer was performed using pure metals (monochromatic Al Kα: Cu $2p_{3/2}$ at 932.62 eV, Au $4f_{7/2}$ at 83.96 eV).[60] Binding energies of elemental lines of the samples are charge referenced to O 1s (oxide) at 530.0 eV. The background pressure in the analysis chamber was

about 7×10^{-8} Pa. Samples were prepared by pressing the wet paste from a 2 ml centrifuge tube onto indium foil and then transferred with a vacuum vessel (PHI model V5000-K) from the glove box into the XPS entry chamber, where pumping overnight removed associated water.

X-ray absorption fine-structure (XAFS) spectroscopy: XAFS spectra were collected at The Rossendorf Beamline at the European Synchrotron Radiation Facility (ESRF, Grenoble). Its experimental station is a dedicated α-laboratory to measure actinides in double confinement sample holders. The energy of the X-ray beam was tuned by a double-crystal monochromator operating in channel-cut mode using a Si(111) crystal pair. Two platinum-coated Si mirrors before and after the monochromator were used to collimate the beam into the monochromator and to reject higher harmonics. Pu L_3-edge spectra were collected in fluorescence mode using a 13-element energy-dispersive solid-state Ge detector (Canberra) together with a digital signal processing unit (XIA XMap). Spectra were collected at 15 K using a closed cycle He cryostat (CryoVac). Energy calibration was performed using the zero crossing of the second derivative of the K-edge of metallic Zr (17998 eV) measured simultaneously to the sample scans. Dead time correction of the fluorescence signal, energy calibration and the averaging of the individual scans were performed with the software package SixPack.[61] Normalization, transformation from energy into k-space, subtraction of a spline background and shell fits were performed with WinXAS following standard procedures.[62] All fits were carried out in R-space (1 to 5 Å) of k^3 –weighted spectra using theoretical backscattering amplitudes and phase shifts calculated with FEFF 8.2[63] on clusters (R_{max} = 8 Å) derived from magnetite[58] and pyrochlore[64] structures, placing Pu into the central 6-coordinated Fe and 8-coordinated lanthanide position, respectively. Debye-Waller factor were restricted to float between 0.002 $Å^{-1}$ and 0.015 $Å^{-1}$. Furthermore, spectra were analyzed by Iterative transformation factor analysis (ITFA).[65]

RESULTS AND DISCUSSION

The initial aim of this study was to investigate the potential uptake of Pu(III) and Pu(V) by magnetite during coprecipitation. No matter if the starting solution contained Pu(III) or Pu(V), however, a final Pu oxidation state of III was established within less than a minute at $pH_{exp} \approx$ 1.5, after mixing with the Fe(II)-Fe(III) solution (Fig. 2). Therefore, Pu(V) was reduced directly to Pu(III) without forming a stable Pu(IV) intermediate, and the reduction was far too rapid for even a kinetically controlled incorporation of Pu(V) during formation of magnetite under strongly reducing conditions. By raising the pH to about 12.5 to induce magnetite precipitation, the Pu concentration dropped below the LSC detection limit of 10^{-9} M (corresponding to a solid liquid distribution ratio, $\log K_d$, > 5.5) suggesting either an efficient retention process associated to the magnetite precipitation, or a rapid Pu(III) precipitation through hydrolysis.[66, 67] After the Fe-inforced recrystallization process, the Pu concentration remained below the LSC detection limit suggesting at a first glance no change of the retention mechanism.

In order to investigate the Pu oxidation state and the local structure in the fresh and recrystallized magnetite samples, we conducted Pu L_{III}-edge XAFS spectroscopy (Fig. 1). The X-ray Absorption Near-Edge Structure (XANES) spectra of all samples show a white line at 18063 eV well aligned in energy and shape with those of aqueous Pu(III) and with Pu(III) sorbed to magnetite (Fig. 3 a).[35] The white lines of aqueous Pu(IV) and Pu(V) reference samples[68] occur at significantly higher energies, and that of Pu(V) shows furthermore the typical shape characteristic of the trans-dioxo (-yl) configuration on the right-wing side of the white line. Therefore, the trivalent oxidation initially present in solution is well preserved after coprecipitation. Linear combination fitting of the spectra confirmed that eventual contributions from oxidation states IV and V are absent or below 2 % (not shown). Formation of PuO_2 associated to the solid phase can further be excluded by XPS, since the corresponding satellite

peak around 432 eV is absent and only the $4f_{7/2}$ peak at 425.2 eV in close agreement with Pu(III) reference samples is present (Supporting Information).

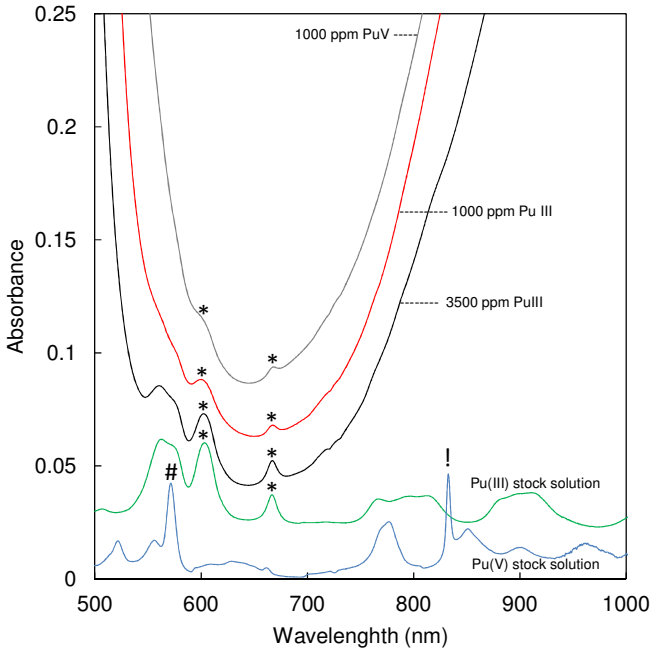

Fig. 2. UV-vis spectra of Pu(III) and Pu(V) stock solutions and of the mixed Fe(II)/Fe(III)/Pu solutions before co-precipitation. "*" marks the absorption peaks used to identify the Pu(III) oxidation state and its concentration. "#" the indicates absorption peaks used to identify the Pu(V) oxidation state and its concentration. "!" indicates absorption peaks used to identify Pu(VI). For clarity, the spectrum of the Pu(V) stock solution is rescaled by a factor of 2, the spectrum of the Pu(III) stock solution is rescaled by a factor of 0.5 and shifted by 0.02 absorption units. The spectra of the Fe(II)/Fe(III)/Pu solutions are shift by 0, 0.005 and 0.02 absorption units for 4400 ppm Pu(III), 1300 ppm Pu(III) and 1300 ppm Pu(V).

The Extended X-ray Absorption Fine-Structure (EXAFS) spectra and their Fourier transform magnitudes (FTM), which represent pseudo-radial distribution functions of the atomic neighbors of Pu, with the distances deviating by about 0.4 Å due to the phase shift Φ, are shown in Fig. 3 b) and c) respectively. The two spectra collected after the recrystallization procedure

(Pu-Mag-1300-rec and Pu-Mag-4400-rec) are very similar to each other and resemble that of the Pu(III) magnetite sorption sample, suggesting that Pu(III) prevails as the tridentate sorption complex previously identified.[35] The spectra of the two fresh coprecipitation samples (Pu-Mag-1300 and Pu-Mag-4400), however, have weaker Pu-O and Pu-$Fe_{1,2}$ FTM peaks in comparison to the sorption complex, suggesting a more distorted local environment or the presence of several Pu species with differing local structures.

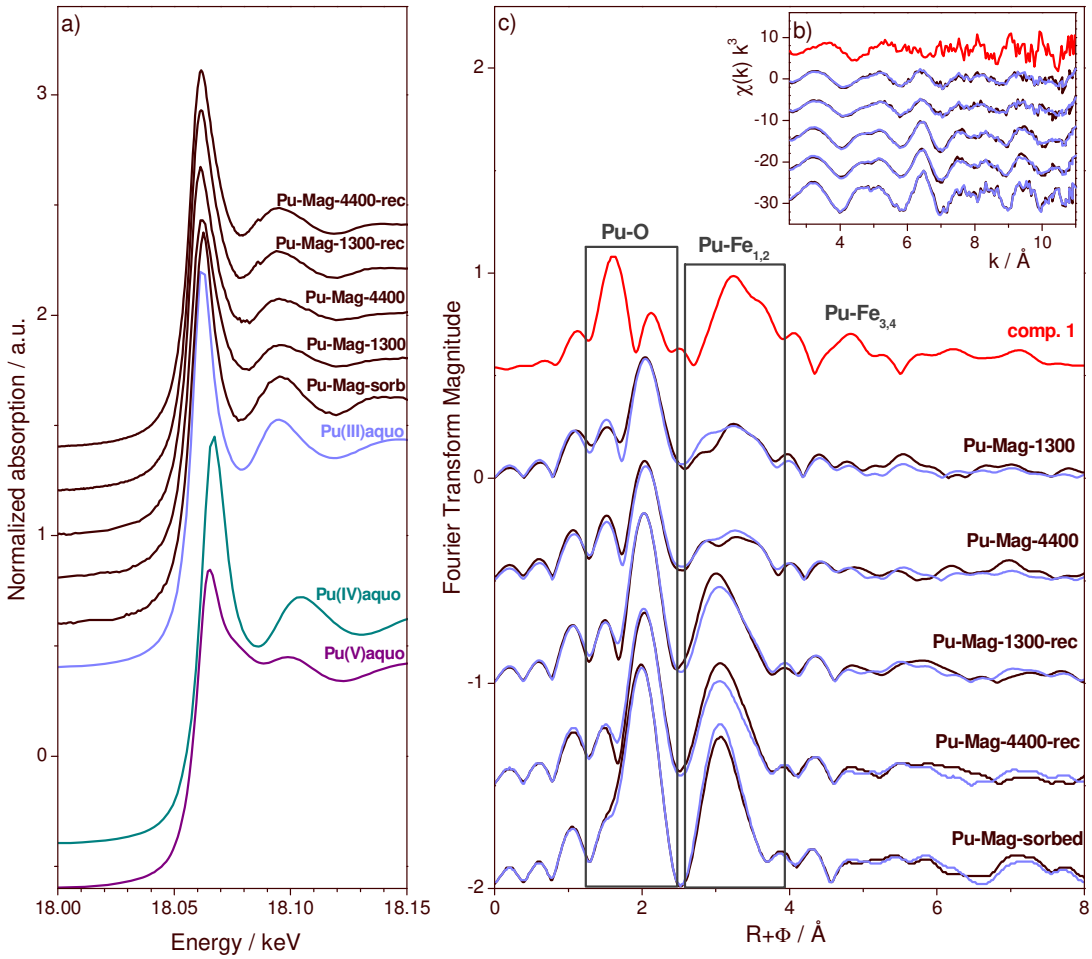

Fig. 3. Pu L_{III} edge XAFS spectra of magnetite coprecipitation samples and selected references. a) XANES spectra, b) k^3-weighted EXAFS spectra, c) corresponding Fourier Transform Magnitudes. For b) and c), black lines are experimental data, and blue lines are ITFA-derived reproductions by two components. Using Pu-Mag-sorb (bottom) as one

endmember component, the second endmember component (comp. 1) was extracted from the full data set (see text). _ENREF_45

In order to determine the short range structure of the fresh coprecipitation samples, we attempted shell fitting based on the magnetite structure, where we replaced Fe in octahedral position by Pu. As expected from the large size difference between Fe and Pu(III) cations, the spectra of Pu-Mag-1300 and Pu-Mag-4400 could not be fit with this approach. Several other fit approaches using single or split Pu-O and Pu-Fe shells did not provide satisfactory results because of (1) poor spectral reproduction (approach 1 in Table SI-1, Fig. SI-4 top,), (2) oxygen coordination numbers of > 12 and hence far higher than those expected for octahedral magnetite positions (6) or the typical tricapped prismatic coordination of trivalent lanthanide and actinide aquo-complexes (9) (approaches 2 and 3 in Table SI-1, Fig. SI-4 center and bottom), and (3) Debye-Waller factors hitting the upper and lower limit of a physically reasonable range (0.002 and 0.015 $Å^2$). Furthermore, wavelet analysis[69] of the Fourier peak around 3 Å clearly revealed the presence of backscattering from a medium-heavy atom like Fe, and not from a heavy atom like Pu, excluding for instance the formation of Pu_2O_3 with Pu-Pu distances of 3.62 and 4.16 Å.[70] Therefore, we had to assume the existence of two or more coexisting Pu species, which cannot be resolved by shell fitting because of the limited resolution (≥0.17 Å at the given k range of 2 to 11 $Å^{-1}$). In such cases, iterative transformation factor analysis (ITFA) has shown to be a valuable approach to determine the number of spectral components (often commensurate to number of species), and to extract the spectra of the pure endmember species.[31, 65] In fact, the spectra of all four precipitation samples are well reproduced by only two components (compare blue and black traces in Fig. 3 b,c), suggesting that two structurally distinguishable Pu species are present in these samples. Furthermore, adding the spectrum of Pu(III) sorbed to magnetite (Pu-Mag-sorb) to the other four spectra did not increase the number of significant components, which indicates that this species is indeed one of the two components, as already suggested by

the spectral similarity with the two re-crystallized samples. Using this information, we could extract the spectrum of the other, unknown component ("comp. 1" shown as top red trace in Fig. 3 b,c) and calculated the fractions of the two species in each sample spectrum (Fig. 4 left). Surprizingly, the fresh precipitates contain already 50% of component 2, the Pu(III) sorption complex, and its percentage even increases with the recrystallization procedure to about 70%. Therefore, even the spectra of the fresh precipitates contain only 50% contribution from component 1, which explains the failure of shell fitting for solving its structure. When using the ITFA-extracted spectrum of component 1, however, we could fit all shells out to a distance of 5.5 Å (R+Φ), well reproducing the EXAFS chi function as well as magnitude and imaginary parts of the Fourier transform (Fig. 4 right). The fit parameters are given in Table 1.

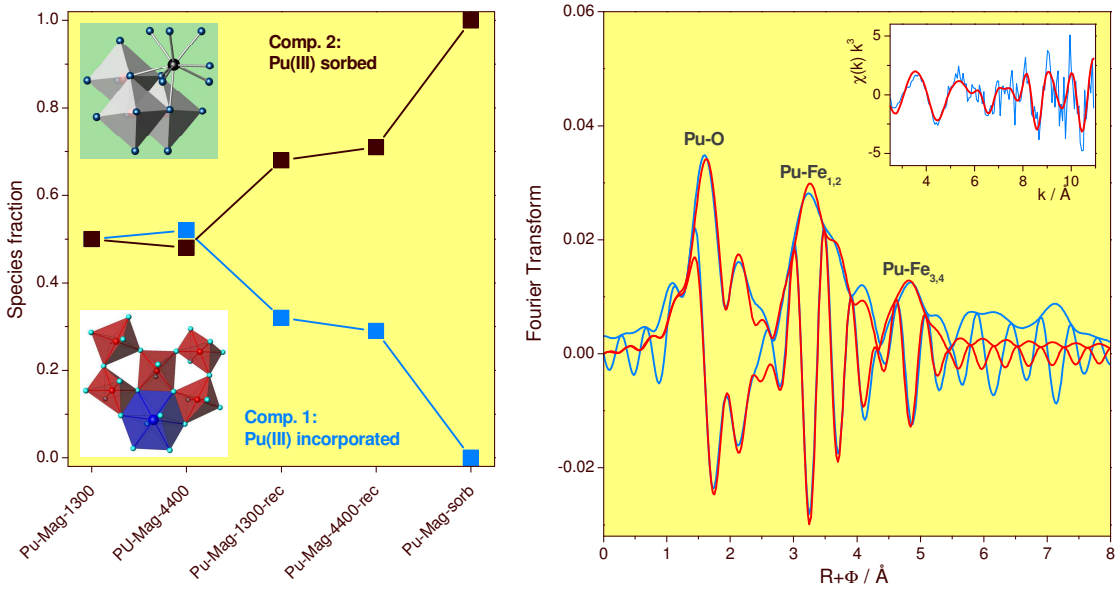

Fig. 4. Left: ITFA-derived relative concentrations of component 1 and 2 in each sample. Component 1 corresponds to Pu(III) incorporated into the magnetite structure, component 2 corresponds to the Pu(III) sorption complex on magnetite. Right: EXAFS shell fit of

component 1 (experimental data: blue lines, best-fit: red line) shown as Fourier transform magnitude and imaginary part, as well as k^3 weighted EXAFS spectra (insert).

Table 1**.** EXAFS shell fit parameters for component 1 along with the crystallographic data for the Fe-occupied Oh site in magnetite and the local structure of component 2 (sorbed Pu(III)) taken from Kirsch et al.[35]

	Component 1 Incorporated Pu(III)					Magnetite Oh site #		Component 2 Sorbed Pu(III)	
Paths	CN	R/Å	σ^2/Å^2	ΔE_0/eV	χ_{res}/%	CN	R/Å	CN	R/Å
Pu-O_1	4.5	2.22	0.0089[a]	8.4	11.1	6	2.06		
Pu-O_2	3.8	2.45	0.0089[a]					9	2.45
Pu-Fe_1	2.7	3.68	0.0032[b]			6	2.95	3	3.54
Pu-Fe_2	1.9	3.93	0.0032[b]			6	3.46	3	4.20
Pu-Fe_3	12*	5.17	0.0150[c]			12	5.11		
Pu-Fe_4	8*	5.47	0.0150[c]			8	5.42		

Superscripts a, b, c, and d indicate correlated parameters

In component 1, Pu(III) coordinates to about 8 oxygen atoms at two different distances, 2.22 and 2.45 Å. Not surprisingly because of the size mismatch between Pu(III) and Fe(II,III), this coordination is very different from the 6-coordinated Fe site in magnetite with a much smaller Fe-O distance of 2.06 Å. The larger distance of 2.45 Å is identical to that of the Pu(III) aquo ion and sorption complexes with 9-fold oxygen coordination.[35] The split shell with an additional shorter Pu-O distance suggests, however, a coordination environment much more distorted than in the trigonal tricapped prism arrangement typical for trivalent lanthanides and actinides in aqueous environment, where the variation of bond distances is commonly too small to be resolved by EXAFS.

Typical oxide structures capable of hosting both large (~1 Å), trivalent lanthanides and actinides alongside much smaller transition metal cations are pyrochlores and perovskites.[71] In perovskites with the general formula ABO_3, the large cation site A is coordinated to 12 oxygen atoms, which significantly deviates from the observed 8-fold coordination for Pu. In pyrochlores with the general formula $A_2B_2O_7$, however, the large A cation is coordinated to 8 oxygen atoms, well matching the fit value (Table 1). Furthermore, in most pyrochlores the A site typically deviates strongly from the perfect cubic coordination, causing a strongly split coordination shell.[64, 72] For instance in a pyrochlore with the trivalent cations Eu, Fe and Ti, hence with cations of very similar diameter, Eu(III) is coordinated to 8 oxygen atoms at 2.20 and 2.48 Å, distances well in line with those in component 1 (structure in lower left corner of Fig. 4 left).[64] The shortest fitted Pu-Fe_1 distance of 3.68 Å corresponds also fairly well with the shortest Eu-Fe distance of 3.60 Å, arising from the edge-sharing linkage between Eu-hosting polyhedra and the nearest Fe-hosting octahedra in pyrochlore. The next shell of Fe atoms (Pu-Fe_2) occurs at a distance of 3.93 Å, which suggests that their octahedra are linked to the actinide polyhedra through corners with a strongly bent Pu-O-Fe axis. Finally, the fitted two long Pu-Fe distances of 5.17 and 5.47 Å do not occur in the pyrochlore structure; they correspond instead reasonably well with (only 0.05 to 0.06 Å longer) Fe-Fe distances in magnetite and are well fit with corresponding coordination numbers of 12 and 8, respectively (Table 1). The absence of the longer-range order of pyrochlore contradict that a separate pyrochlore phase trapped Pu (note that the small amount of this phase may not be detectable by XRD). Based on these fitted shell distances and coordination numbers, the structure of component 1 can hence be conceptualized as Pu(III) entrapped in magnetite by adopting a pyrochlore-like structure with a radius of less than 4 Å, which is embedded in the magnetite structure seen beyond 5 Å.

This experimental data is in clear contradiction to the result of a recent quantum mechanical approach, where structural incorporation into the Oh site of magnetite was predicted.[73]

Furthermore, it also does not confirm a postulated 6-fold coordination for Am in magnetite after 2 years of aging at a pH ~12,[49] where shell fitting might have been biased by a mix of sorbed and occludesd Am species similar to our results before separating their spectra contributions with ITFA. It is well in line, however, with Sm(III) in Sm-doped magnetite being in 8-fold coordination.[48] In this study, unfortunately only very short Sm L-edge EXAFS spectra could be collected due to the following Fe K-edge (up to 8.5 $Å^{-1}$), inhibiting analysis of shells beyond the first coordination sphere.

CONCLUSION

Our results show that under the given experimental conditions Pu(V) in a mixed solution of Fe(II) and Fe(III) under anoxic conditions is rapidly reduced to Pu(III), confirming the relevance of this oxidation state previously suggested by thermodynamic data and experiments.[35] The base-induced precipitation product is pure magnetite, which partitions Pu(III) partly by structural incorporation, partly by surface complexation. In the fresh precipitate, both retention mechanisms occur in about equal fractions and are independent of the Pu loading; after the Fe-inforced recrystallization, the sorption complex prevails (about 2/3 versus 1/3 incorporation), again independent of Pu loading. Therefore, the process is controlled by the magnetite crystallization and recrystallization mechanisms and kinetics, and not by Pu(III) dependent parameters.

In all four samples, the calculated retention coefficient for Pu, logKd, is larger than 5.5, testimony of the strong Pu retention by both mechanisms at two pH values (12.5 for the fresh, 6.5 for the recrystallized samples). Nevertheless, structural incorporation into magnetite, a phase which is stable across a relatively wide geochemical parameter field, may provide a better protection against Pu-remobilization in case of changing groundwater chemistry, like increasing Eh or decreasing pH, in comparison to sorption at the magnetite surface as has been

demonstrated for instance for Tc(IV).[74, 75]. Therefore, the question whether or not the entrapped Pu species represents a thermodynamically stable phase, is of substantial interest. In nature, lanthanides are hosted prevalently by minerals with pyrochlore or perovskite structures, where eight- or nine-coordinated sites offer more space for their large ionic radii than octahedral sites.[71, 76] Pyrochlores are also considered as stable waste forms for actinide and lanthanide radionuclides because of the structure's high tolerance of accommodating defects and disorder, including those induced by heavy internal alpha irradiation.[72, 77, 78] Here, however, we have no evidence for the formation of such a separate phase, but for the formation of small clusters with 8 Å diameter embedded in the magnetite structure, suggesting that the incorporation of Pu(III) into magnetite can only be achieved by a substantial restructuring of the local environment, which may cause structural strain and subsequent expulsion of Pu from the structure. The increase of the sorbed Pu fraction after recrystallization points into this direction. Plutonium uptake into the structure would then be a kinetically driven process (kinetic entrapment), followed by thermodynamically driven expulsion from the structure. While this process provides an intriguing explanation of our observations, we have no proper proof for this, since we also changed the pH during the re-crystalization from 12.5 to 6.5 to better mimick long-term conditions in the nuclear waste repository.[79] Therefore, we cannot exclude that also the pH and [Fe^{II}] changes in the recrystallization experiment enhanced the solid/liquid ion exchange and Fe(II) and Pu(III) solubility, which accelerated Pu(III) to be expelled from the host magnetite.[66, 67, 80, 81]

Since Fe(II) concentration and pH used in the recrystallization step is similar to the geochemical settings in the near-field of anoxic deep-underground repositories hosting nuclear waste in steel containers, our recrystallization experiment provides evidence that structural incorporation of Pu(III) is less favorable under such conditions than surface complexation and should be considered for the safety case.

ACKNOWLEDGEMENT: This project was financially supported by BMBF project 02NUK019D and the European FP7 project TALISMAN (Transnational Access to Large Infrastructure for the Safe MAnagement of Actinides). The wet-chemistry work was performed in the controlled area of KIT-INE with support of KIT-INE technical staff, and the XAFS studies were performed at The Rossendorf Beamline at ESRF (BM20).

SUPPORTING INFORMATION. XPS data and additional EXAFS shell fits of sample Pu-Mag-1300

REFERENCES

1. Choppin, G. R. Actinide speciation in the environment. *Radiochimica Acta* **2003,** *91*, 645-650.

2. Kaplan, D. I.; Demirkanli, D. I.; Gumapas, L.; Powell, B. A.; Fjeld, R. A.; Molz, F. J.; Serkiz, S. M. Eleven-year field study of Pu migration from PuIII, IV, and VI sources. *Environmental Science & Technology* **2006,** *40* (2), 443-448.

3. Kaplan, D. I.; Powell, B. A.; Demirkanli, D. I.; Fjeld, R. A.; Molz, F. J.; Serkiz, S. M.; Coates, J. T. Influence of oxidation states on plutonium mobility during long-term transport through an unsaturated subsurface environment. *Environmental Science & Technology* **2004,** *38* (19), 5053-5058.

4. Kaplan, D. I.; Powell, B. A.; Gumapas, L.; Coates, J. T.; Fjeld, R. A.; Diprete, D. P. Influence of pH on plutonium desorption/solubilization from sediment. *Environmental Science & Technology* **2006,** *40* (19), 5937-5942.

5. Duff, M. C.; Newville, M.; Hunter, D. B.; Bertsch, P. M.; Sutton, S. R.; Triay, I. R.; Vaniman, D. T.; Eng, P.; Rivers, M. L. Micro-XAS studies with sorbed plutonium on tuff. *Journal of Synchrotron Radiation* **1999,** *6*, 350-352.

6. Kersting, A. B.; Efurd, D. W.; Finnegan, D. L.; Rokop, D. J.; Smith, D. K.; Thompson, J. L. Migration of plutonium in ground water at the Nevada Test Site. *Nature* **1999,** *397*, 56-59.

7. Novikov, A. P.; Kalmykov, S. N.; Utsunomiya, S.; Ewing, R. C.; Horreard, F.; Merkulov, A.; Clark, S. B.; Tkachev, V. V.; Myasoedov, B. F. Colloid transport of plutonium in the far-field of the Mayak Production Association, Russia. *Science* **2006,** *314*, 638-641.

8. Jeanson, A.; Berthon, C.; Coantic, S.; Den Auwer, C.; Floquet, N.; Funke, H.; Guillaneux, D.; Hennig, C.; Martinez, J.; Moisy, P.; Petit, S.; Proux, O.; Quemeneur, E.; Solari, P. L.; Subra, G. The role of aspartyl-rich pentapeptides in comparative complexation of actinide(IV) and iron(III). Part 1. *New Journal of Chemistry* **2009,** *33* (5), 976-985.

9. Jeanson, A.; Ferrand, M.; Funke, H.; Hennig, C.; Moisy, P.; Solari, P. L.; Vidaud, C.; Den Auwer, C. The Role of Transferrin in Actinide(IV) Uptake: Comparison with Iron(III). *Chemistry-a European Journal* **2010,** *16* (4), 1378-1387.

10. Marquardt, C. M.; Seibert, A.; Artinger, R.; Denecke, M. A.; Kuczewski, B.; Schild, D.; Fanghanel, T. The redox behaviour of plutonium in humic rich groundwater. *Radiochimica Acta* **2004,** *92* (9-11), 617-623.

11. Moll, H.; Merroun, M. L.; Hennig, C.; Rossberg, A.; Selenska-Pobell, S.; Bernhard, G. The interaction of Desulfovibrio äspöensis DSM 10631T with plutonium. *Radiochimica Acta* **2006,** *94*, 815-824.

12. Neu, M. P.; Icopini, G. A.; Boukhalfa, H. Plutonium speciation affected by environmental bacteria. *Radiochimica Acta* **2005,** *93* (11), 705-714.

13. Schmeide, K.; Reich, T.; Sachs, S.; Bernhard, G. Plutonium(III) complexation by humic substances studied by X-ray absorption fine structure spectroscopy. *Inorganica Chimica Acta* **2006,** *359* (1), 237-242.

14. Metz, V.; Geckeis, H.; Gonzalez-Robles, E.; Loida, A.; Bube, C.; Kienzler, B. Radionuclide behaviour in the near-field of a geological repository for spent nuclear fuel. *Radiochimica Acta* **2012,** *100* (8-9), 699-713.

15. Schlegel, M. L.; Bataillon, C.; Blanc, C.; Pret, D.; Foy, E. Anodic activation of iron corrosion in clay media under water-saturated conditions at 90 degrees C: Characterization of the corrosion interface. *Environmental Science & Technology* **2010,** *44* (4), 1503-1508.

16. Wersin, P.; Jenni, A.; Mader, U. K. Interaction of corroding iron with bentonite in the ABM1 experiment at Aspo, Sweden: A microscopic approach. *Clays and Clay Minerals* **2015,** *63* (1-2), 51-68.

17. Grambow, B.; Smailos, E.; Geckeis, H.; Muller, R.; Hentschel, H. Sorption and reduction of uranium(VI) on iron corrosion products under reducing saline conditions. *Radiochimica Acta* **1996,** *74*, 149-154.

18. El Hajj, H.; Abdelouas, A.; El Mendili, Y.; Karakurt, G.; Grambow, B.; Martin, C. Corrosion of carbon steel under sequential aerobic-anaerobic environmental conditions. *Corrosion Science* **2013,** *76*, 432-440.

19. Singer, D. M.; Chatman, S. M.; Ilton, E. S.; Rosso, K. M.; Banfield, J. F.; Waychunas, G. A. U(VI) Sorption and Reduction Kinetics on the Magnetite (111) Surface. *Environmental Science & Technology* **2012,** *46* (7), 3821-3830.

20. Singer, D. M.; Chatman, S. M.; Ilton, E. S.; Rosso, K. M.; Banfield, J. F.; Waychunas, G. A. Identification of Simultaneous U(VI) Sorption Complexes and U(IV) Nanoprecipitates on the Magnetite (111) Surface. *Environmental Science & Technology* **2012,** *46* (7), 3811-3820.

21. Cevirim-Papaioannou, N.; Yalcintas, E.; Gaona, X.; Dardenne, K.; Altmaier, M.; Geckeis, H. Redox chemistry of uranium in reducing, dilute to concentrated NaCl solutions. *Applied Geochemistry* **2018,** *98*, 286-300.

22. Bruno, J.; González-Siso, M. R.; Duro, L.; Gaona, X.; Altmaier, M. *Key master variables affecting the mobility of Ni, Pu, Tc and U in the near field of the SFR repository*; 2018.

23. Latta, D. E.; Gorski, C. A.; Boyanov, M. I.; O'Loughlin, E. J.; Kemner, K. M.; Scherer, M. M. Influence of Magnetite Stoichiometry on U-VI Reduction. *Environmental Science & Technology* **2012,** *46* (2), 778-786.

24. Scheinost, A. C.; Steudtner, R.; Hübner, R.; Weiss, S.; Bok, F. Neptunium^{V} retention by siderite under anoxic conditions: Precipitation of NpO_2−like nanoparticles and of Np^{IV} pentacarbonate. *Environ. Sci. Technol.* **2016,** *50*, 10413-10420.

25. Nakata, K.; Nagasaki, S.; Tanaka, S.; Sakamoto, Y.; Tanaka, T.; Ogawa, H. Reduction rate of neptunium(V) in heterogeneous solution with magnetite. *Radiochimica Acta* **2004,** *92* (3), 145-149.

26. Fellhauer, D. Untersuchungen zur Redoxchemie und Löslichkeit von Neptunium und Plutonium. PhD, University of Heidelberg, Germany, 2013.

27. Charlet, L.; Scheinost, A. C.; Tournassat, C.; Greneche, J. M.; Géhin, A.; Fernández-Martínez, A.; Coudert, S.; Tisserand, D.; Brendle, J. Electron transfer at the mineral/water

interface: Selenium reduction by ferrous iron sorbed on clay. *Geochimica et Cosmochimica Acta* **2007**, submitted.

28. Scheinost, A. C.; Charlet, L. Selenite reduction by mackinawite, magnetite and siderite: XAS characterization of nanosized redox products. *Environ. Sci. Technol.* **2008,** *42* (6), 1984–1989.

29. Scheinost, A. C.; Kirsch, R.; Banerjee, D.; Fernandez-Martinez, A.; Zaenker, H.; Funke, H.; Charlet, L. X-ray absorption and photoelectron spectroscopy investigation of selenite reduction by FeII-bearing minerals. *Journal of Contaminant Hydrology* **2008,** *102*, 228-245.

30. Kobayashi, T.; Scheinost, A. C.; Fellhauer, D.; Gaona, X.; Altmaier, M. Redox behavior of Tc(VII)/Tc(IV) under various reducing conditions in 0.1 M NaCl solutions. *Radiochimica Acta* **2013,** *101* (5), 323-332.

31. Yalçıntaş, E.; Scheinost, A. C.; Gaona, X.; Altmaier, M. Systematic XAS study on the reduction and uptake of Tc by magnetite and mackinawite. *Dalton Trans.* **2016,** *45*, 17874-17885.

32. Powell, B. A.; Fjeld, R. A.; Kaplan, D. I.; Coates, J. T.; Serkiz, S. M. $Pu(V)O_2^+$ adsorption and reduction by synthetic magnetite (Fe_3O_4). *Environmental Science & Technology* **2004,** *38* (22), 6016-6024.

33. Powell, B. A.; Fjeld, R. A.; Kaplan, D. I.; Coates, J. T.; Serkiz, S. M. $Pu(V)O_2^+$ adsorption and reduction by synthetic hematite and goethite. *Environmental Science & Technology* **2005,** *39* (7), 2107-2114.

34. Romanchuk, A. Y.; Kalmykov, S. N.; Aliev, R. A. Plutonium sorption onto hematite colloids at femto- and nanomolar concentrations. *Radiochimica Acta* **2011,** *99* (3), 137-144.

35. Kirsch, R.; Fellhauer, D.; Altmaier, M.; Neck, V.; Rossberg, A.; Fanghänel, T.; Charlet, L.; Scheinost, A. C. Oxidation state and local structure of plutonium reacted with magnetite, mackinawite and chukanovite. *Environmental Science & Technology* **2011,** *45* (17), 7267–7274.

36. Shannon, R. D. Revised effective ionic radii and systematic studies of interatomic distances in halides and chalcogenides. *Acta Crystallogr. Sect. A* **1976,** *32* (SEP1), 751-767.

37. Dulnee, S.; Banerjee, D.; Merkel, B. J.; Scheinost, A. C. Surface complexation and oxidation of Sn^{II} by nanomagnetite. *Environ. Sci. Technol.* **2013,** *47* (22), 12852–12859.

38. Stewart, B. D.; Nico, P. S.; Fendorf, S. Stability of Uranium Incorporated into Fe (Hydr)oxides under Fluctuating Redox Conditions. *Environmental Science & Technology* **2009,** *43* (13), 4922-4927.

39. Nico, P. S.; Stewart, B. D.; Fendorf, S. Incorporation of Oxidized Uranium into Fe (Hydr)oxides during Fe(II) Catalyzed Remineralization. *Environmental Science & Technology* **2009,** *43* (19), 7391-7396.

40. Pidchenko, I.; Kvashnina, K. O.; Yokosawa, T.; Finck, N.; Bahl, S.; Schild, D.; Polly, R.; Bohnert, E.; Rossberg, A.; Gottlicher, J.; Dardenne, K.; Rothe, J.; Schafer, T.; Geckeis, H.; Vitova, T. Uranium Redox Transformations after U(VI) Coprecipitation with Magnetite Nanoparticles. *Environmental Science & Technology* **2017,** *51* (4), 2217-2225.

41. De Silva, C. R.; Smith, S.; Shim, I.; Pyun, J.; Gutu, T.; Jiao, J.; Zheng, Z. P. Lanthanide(III)-doped magnetite nanoparticles. *Journal of the American Chemical Society* **2009,** *131* (18), 6336-+.

42. Moon, J. W.; Roh, Y.; Yeary, L. W.; Lauf, R. J.; Rawn, C. J.; Love, L. J.; Phelps, T. J. Microbial formation of lanthanide-substituted magnetites by Thermoanaerobacter sp TOR-39. *Extremophiles* **2007,** *11* (6), 859-867.

43. Kahn, M. L.; Zhang, Z. J. Synthesis and magnetic properties of CoFe2O4 spinel ferrite nanoparticles doped with lanthanide ions. *Appl. Phys. Lett.* **2001,** *78* (23), 3651-3653.

44. Drake, P.; Cho, H. J.; Shih, P. S.; Kao, C. H.; Lee, K. F.; Kuo, C. H.; Lin, X. Z.; Lin, Y. J. Gd-doped iron-oxide nanoparticles for tumour therapy via magnetic field hyperthermia. *J. Mater. Chem.* **2007,** *17* (46), 4914-4918.

45. Sattar, A. A.; ElShokrofy, K. M. Rare earth doping effect on the electrical properties of Cu-Zn ferrites. *J. Phys. IV* **1997,** *7* (C1), 245-246.

46. Zhang, H. H.; Malik, V.; Mallapragada, S.; Akinc, M. Synthesis and characterization of Gd-doped magnetite nanoparticles. *Journal of Magnetism and Magnetic Materials* **2017,** *423*, 386-394.

47. Park, J. C.; Yeo, S.; Kim, M.; Lee, G. T.; Seo, J. H. Synthesis and characterization of novel lanthanide-doped magnetite@Au core@shell nanoparticles. *Materials Letters* **2016,** *181*, 272-277.

48. Soldatov, M. A.; Martini, A.; Bugaev, A. L.; Pankin, I.; Medvedev, P. V.; Guda, A. A.; Aboraia, A. M.; Podkovyrina, Y. S.; Budnyk, A. P.; Soldatov, A. A.; Lamberti, C. The insights from X-ray absorption spectroscopy into the local atomic structure and chemical bonding of Metal-organic frameworks. *Polyhedron* **2018,** *155*, 232-253.

49. Finck, N.; Nedel, S.; Dideriksen, K.; Schlegel, M. L. Trivalent actinide uptake by iron (hydr)oxides. *Environmental Science & Technology* **2016,** *50* (19), 10428-10436.

50. Boland, D. D.; Collins, R. N.; Payne, T. E.; Waite, T. D. Effect of Amorphous Fe(III) Oxide Transformation on the Fe(II)-Mediated Reduction of U(VI). *Environmental Science & Technology* **2011,** *45* (4), 1327-1333.

51. Catalano, J. G.; Fenter, P.; Park, C.; Rosso, K. M.; Frierdich, A. J.; Otemuyiwa, B. T. Fe(II)-induced structural transformations of hematite surfaces and their impact on contaminants. *Geochimica Et Cosmochimica Acta* **2010,** *74* (12), A150-A150.

52. Handler, R. M.; Beard, B. L.; Johnson, C. M.; Scherer, M. M. Atom Exchange between Aqueous Fe(II) and Goethite: An Fe Isotope Tracer Study. *Environmental Science & Technology* **2009,** *43* (4), 1102-1107.

53. Pedersen, H. D.; Postma, D.; Jakobsen, R.; Larsen, O. Fast transformation of iron oxyhydroxides by the catalytic action of aqueous Fe(II). *Geochimica Et Cosmochimica Acta* **2005,** *69* (16), 3967-3977.

54. Jones, A. M.; Collins, R. N.; Rose, J.; Waite, T. D. The effect of silica and natural organic matter on the Fe(II)-catalysed transformation and reactivity of Fe(III) minerals. *Geochimica Et Cosmochimica Acta* **2009,** *73* (15), 4409-4422.

55. Wan, J.; Cai, W.; Meng, X.; Liu, E. Monodisperse water-soluble magnetite nanoparticles prepared by polyol process for high-performance magnetic resonance imaging. *Chemical Communications* **2007,** (47), 5004-5006.

56. Wang, J.; Deng, T.; Dai, Y. J. Study on the processes and mechanism of the formation of Fe3O4 at low temperature. *Journal of Alloys and Compounds* **2005,** *390* (1-2), 127-132.

57. Viollier, E.; Inglett, P. W.; Hunter, K.; Roychoudhury, A. N.; Van Cappellen, P. The ferrozine method revisited: Fe(II)/Fe(III) determination in natural waters. *Applied Geochemistry* **2000,** *15* (6), 785-790.

58. Wright, J. P.; Attfield, J. P.; Radaelli, P. G. Charge ordered structure of magnetite Fe3O4 below the Verwey transition. *Phys Rev B* **2002,** *66* (21).

59. Chtoun, E. H.; Hanebali, L.; Garnier, P. X-ray Rietveld analysis of (1-x)$A_2Ti_2O(7)$-xFe_2TiO_5 (A= Eu,Y) solid solutions. *Ann. Chim.-Sci. Mat.* **2001,** *26* (3), 27-32.

60. Seah, M. P.; Gilmore, L. S.; Beamson, G. XPS: Binding energy calibration of electron spectrometers 5 - Re-evaluation of the reference energies. *Surface and Interface Analysis* **1998,** *26* (9), 642-649.

61. Webb, S. M. Sixpack: a graphical user interface for XAS analysis using IFEFFIT. *Physica Scripta* **2005,** *T115*, 1011-1014.

62. Ressler, T. WinXAS: a program for X-ray absorption spectroscopy data analysis under MS-Windows. *Journal of Synchrotron Radiation* **1998,** *5* (2), 118-122.

63. Ankudinov, A. L.; Rehr, J. J. Relativistic calculations of spin-dependent x-ray-absorption spectra. *Physical Review B* **1997,** *56* (1712-1728).

64. Chtoun, E. H.; Hanebali, L.; Garnier, P. X-ray Rietveld analysis of (1-x)A(2)Ti(2)O(7)-xFe(2)TiO(5) (A= Eu,Y) solid solutions. *Annales De Chimie-Science Des Materiaux* **2001,** *26* (3), 27-32.

65. Rossberg, A.; Reich, T.; Bernhard, G. Complexation of uranium(VI) with protocatechuic acid - application of iterative transformation factor analysis to EXAFS spectroscopy. *Anal. Bioanal. Chem.* **2003,** *376* (5), 631-638.

66. Cho, H.-R.; Youn, Y.-S.; Jung, E. C.; Cha, W. Hydrolysis of trivalent plutonium and solubility of Pu(OH)(3) (am) under electrolytic reducing conditions. *Dalton Transactions* **2016,** *45* (48), 19449-19457.

67. Tasi, A.; Gaona, X.; Fellhauer, D.; Boettle, M.; Rothe, J.; Dardenne, K.; Schild, D.; Grive, M.; Colas, E.; Bruno, J.; Kallstrom, K.; Altmaier, M.; Geckeis, H. Redox behavior and solubility of plutonium under alkaline, reducing conditions. *Radiochimica Acta* **2018,** *106* (4), 259-279.

68. Dalodière, E.; Virot, M.; Dumas, T.; Guillaumont, D.; Illy, M.-C.; Berthon, C.; Guerin, L.; Rossberg, A.; Venault, L.; Moisy, P.; Nikitenko, S. I. Structural and magnetic susceptibility characterization of Pu(V) aqua ion using sonochemistry as a facile synthesis method. *Inorganic Chemistry Frontiers* **2018,** *5*, 100-111.

69. Funke, H.; Scheinost, A. C.; Chukalina, M. Wavelet analysis of extended X-ray absorption fine structure data. *Physical Review* **2005,** *B 71*, 094110.

70. Chikalla, T. D.; McNeilly, C. E.; Skavdahl, R. E. The plutonium-oxygen system. *Journal of Nuclear Materials* **1964,** *12* (2), 131-141.

71. Daniels, L. M. W. Structures and Properties of Perovskites and Pyrochlores from Hydrothermal Synthesis. PhD Thesis, University of Warwick, 2015.

72. Belin, R. C.; Martin, P. M.; Valenza, P. J.; Scheinost, A. C. Experimental insight into the radiation resistance of zirconia-based americium ceramics. *Inorganic Chemistry* **2009,** *48*, 5376-5381.

73. Bender, W. M.; Becker, U. Quantum-mechanical investigation of the structures and energetics of uranium and plutonium incorporated into the magnetite (Fe_3O_4 lattice. *ACS Earth Space Chem.* **2019,** *3*, 637-651.

74. Um, W.; Chang, H. S.; Icenhower, J. P.; Lukens, W. W.; Serne, R. J.; Qafoku, N. P.; Westsik, J. H.; Buck, E. C.; Smith, S. C. Immobilization of 99-Technetium (VII) by Fe(II)-

Goethite and Limited Reoxidation. *Environmental Science & Technology* **2011,** *45* (11), 4904-4913.

75. Marshall, T. A.; Morris, K.; Law, G. T. W.; Mosselmans, J. F. W.; Bots, P.; Parry, S. A.; Shaw, S. Incorporation and Retention of 99-Tc(IV) in Magnetite under High pH Conditions. *Environmental Science & Technology* **2014,** *48* (20), 11853-11862.

76. Rajendran, M.; Bhattacharya, A. K. Nanocrystalline orthoferrite powders: Synthesis and magnetic properties. *J. Eur. Ceram. Soc.* **2006,** *26* (16), 3675-3679.

77. Lumpkin, G. R.; Ewing, R. C. Alpha-decay damage in minerals of the pyrochlore group. *Physics and Chemistry of Minerals* **1988,** *16* (1), 2-20.

78. Wang, S. X.; Begg, B. D.; Wang, L. M.; Ewing, R. C.; Weber, W. J.; Kutty, K. V. G. Radiation stability of gadolinium zirconate: A waste form for plutonium disposition. *Journal of Materials Research* **1999,** *14* (12), 4470-4473.

79. Sellin, P.; Leupin, O. X. The use of clay as an engineered barrier in radioactive waste management - A review. *Clays and Clay Minerals* **2013,** *61* (6), 477-498.

80. Watson, E. B. A conceptual model for near-surface kinetic controls on the trace-element and stable isotope composition of abiogenic calcite crystals. *Geochimica Et Cosmochimica Acta* **2004,** *68* (7), 1473-1488.

81. Thien, B. M. J.; Kulik, D. A.; Curti, E. Modeling trace element uptake kinetics in secondary minerals. In *Proceedings of the Fourteenth International Symposium on Water-Rock Interaction, WRI 14*, Hellmann, R.; Pitsch, H., Eds. Elsevier Science Amsterdam, 2013; Vol. 7, pp 838-841.